2024 IEEE International Conference on Robotics and Automation (ICRA 2024)
May 13-17, 2024. Yokohama, Japan

# A Multi-modal Hybrid Robot with Enhanced Traversal Performance*

Zhipeng He, Na Zhao†, Yudong Luo, Sian Long, Xi Luo, and Hongbin Deng

***Abstract*— Current multi-modal hybrid robots with flight and wheeled modes have fallen into the dilemma that they can only avoid obstacles by re-taking off when encountering obstacles due to the poor performance of wheeled obstacle-crossing. To tackle this problem, this paper presents a novel multi-modal hybrid robot with the ability to actively adjust the wheel's size, which is inspired by the behavior of the turtle's legs when it encounters obstacles, to enhance the traversal performance. In detail, we describe the hardware design that allows the robot to achieve a modal switch between flight and wheeled modes through foldable structures and variable wheel diameters; then, we present the architecture to control these two morphing mechanisms. After that, we establish the theoretical kinematic models for both the foldable arm and variable wheel and carry out extensive experiments to test the performance of the foldable arm, the variable-diameter wheel, as well as the traversal performance of the robot. Experimental results show that the proposed multimodal robot can realize the function of a quadrotor, respond quickly with full-scale folding within 0.9 s, climb a maximum slope of 36°, and traverse narrow passageways, which exhibit superior mobility and environmental adaptability.**

## I. Introduction

Due to the characteristics of small size, superior maneuverability, and wide field of view, UAVs have become an ideal platform for indoor and outdoor applications with a spatial span, such as photographing, surveillance, and search and rescue [1]. However, for confined spaces such as between buildings, pipelines, mine holes, and stairs, UAVs are susceptible to signal loss, environmental obstacles, or the operator's skills. It is challenging for UAVs to stay in reconnaissance for a long time due to limited endurance. In terms of drone safety, the sound emitted by the rotor is too high, leading to low concealment. UGVs, on the other hand, have high payload capability, and can freely stop and go with low noise and low power cost [2]. Multi-modal robots, which are able to switch between UAV and UGV, provide a trade-off solution [3], [4].

The key technology for a multimodal robot is to design a mechanism to realize modal transformation and single-modal operation, primarily achieved by morphing [5], and researchers have synthesized various types of multi-modal robots. In detail, the work [3], [6], [7] has reported a series of "STAR" robots with similar shapes. Their arms are folded downward to achieve modal transition, and the wheels are driven by propeller motors in wheeled mode. However, this wheeled mode coupled with propeller motors could cause significant disturbance to the environment, such as raising dust, increasing noise, easily damaging surrounding objects, increasing body vibration, and increasing the error of onboard sensors. Besides, after the arm is folded, the propeller will generate more lateral force. This force does not contribute to the robot's forward motion, but will increase unnecessary energy consumption. In [6], the propellers are used to generate negative pressure to climb on the wall, but for normal driving, this design could hinder the speed of the robot's movement and the energy consumption increases accordingly. Therefore, the clutch is added to be time-sharing drive propellers and wheels in [7], which has reduced the driving energy consumption by 52% and achieved higher speed. However, the wheels still rotate with the propeller during flight, which undoubtedly increases energy consumption. Additionally, this design was more complex than the first two types.

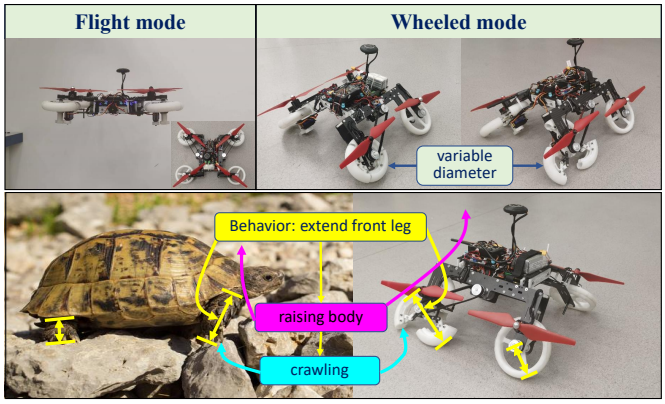


Fig. 1. Prototype of the robot and a source of inspiration to improve the robot's traversing performance.

In addition, the M4 robot [5] adopts a gearbox-driven propeller as the wheel. The leg arm can move sideways, and swing forward and backward. This robot has 22 degrees of freedom and 8 modes, and its massive system increases the complexity of the structure and the difficulty of control. The BogieCopter [8] consists of two tiltable axles and four independent passive wheels, using the same set of drivers for all motion modes. HyTAQ [9] adds a rolling cage wrapped around the entire machine as a passive wheel to perform ground motion based on a quadrotor, increasing additional resistance since the overall shape is easily affected by wind. The robot proposed in [10] employs independent motors to

*This work was supported by the National Natural Science Foundation of China under Grant 52305009 and the Fundamental Research Funds for the Central Universities under Grant 3132023266.

Zhipeng He and Hongbin Deng are with the School of Mechatronical Engineering, Beijing Institute of Technology, Beijing 100081, China.

Na Zhao†, Yudong Luo, and Sian Long are with Morphing Robotics Lab, the Department of Computer Science and Technology, Dalian Maritime University, Dalian, Liaoning 116026, China.

Xi Luo is with Yichang Testing Tech. Research Institution, Yichang, Hubei 410083, China.

†Corresponding author. Email: *zna@dlmu.edu.cn*

drive the wheels. The robot's size is relatively large and not easy to stabilize, as it is prone to rollover when climbing or crossing obstacles. The robot presented in [11] is equipped with additional motors for the ground and a mechanism to fold one side of the arm after landing. The wheels are located in the middle of both sides of the body. When one arm folds, the wheels move at the forefront while traveling on land, and the synchronous belt drives the long arm connected to the back. However, the control system for mode switching is complex and has significant delays. In addition to the above work, there is a lot of outstanding work, such as Drivocopter [12], SytaB [13], LEONARDO [14], [15], Skywalker [16], [17], [18], [19], [20] and [21]. In addition to the above problems such as the modal coupling and system complexity, few works describe the robots in wheeled mode to avoid obstacles on the ground. The most straightforward way is to take off to avoid obstacles, which is more energy-intensive.

To this end, we propose a novel multi-modal robot with enhanced traversing capability while balancing its functionality, endurance, and noise, and reducing complexity in structure and control in the design process. The robot can switch between flight and wheeled modes by actively folding its arms and crossing obstacles with the option of changing the size of the wheels and its mode (wheeled or legged) instead of switching back to flight mode, thus eliminating the energy consumption in modal transitions and activating the propeller motors. Besides, an active drive strategy without coupling with the propeller motors is adopted in the wheels so that when close reconnaissance is required, the robot can move with low noise due to the absence of propellers, thus ensuring safety and reducing energy consumption. In addition, in the wheeled mode, the robot moves normally with small wheels, which can ensure a low center of gravity to maintain stability. This behavior is common in nature, such as turtles [22], sea lions [23], and walruses. Take turtles for an example, see bottom left of Fig. 1, on flat roads, the turtle generally moves by keeping the center of gravity low in the form of short legs to maintain high stability and low energy consumption; while when encountering relatively high obstacles, it will stretch its front legs and raise the body to avoid hitting obstacles beneath its body. At the same time, two front legs grab the obstacles for higher friction to avoid slipping back, and to adapt to unstructured and irregular terrain.

The contributions of this work are threefold. Firstly, we show a flyable and wheeled multi-modal robot with variable-diameter wheels to enhance its traveling performance on the ground, which has not been reported in the literature on multi-modal robots. Secondly, the design for the variable-diameter wheel is modular and scalable, supporting a greater morphing ratio and different sizes of wheels. Thirdly, we construct a systematic hardware and architecture platform and experimentally demonstrate the ability to combine the diversity of modes and wheel sizes to complete various maneuvers, such as traveling over steep ramps and traversal narrow passageways.

This paper is organized as follows. Sec. II presents the overall design of the multi-modal robot, points out the key to designing the robot, and emphasizes the mechanism of the robot in wheeled mode with the architecture of actuation and control. Sec. III constructs the robot's kinematics model, focusing on analyzing the geometric relationship and motion law of the foldable arm and various-diameter wheel. Sec. IV demonstrates the experimental results of testing the robot in different scenarios. Finally, we conclude our work.

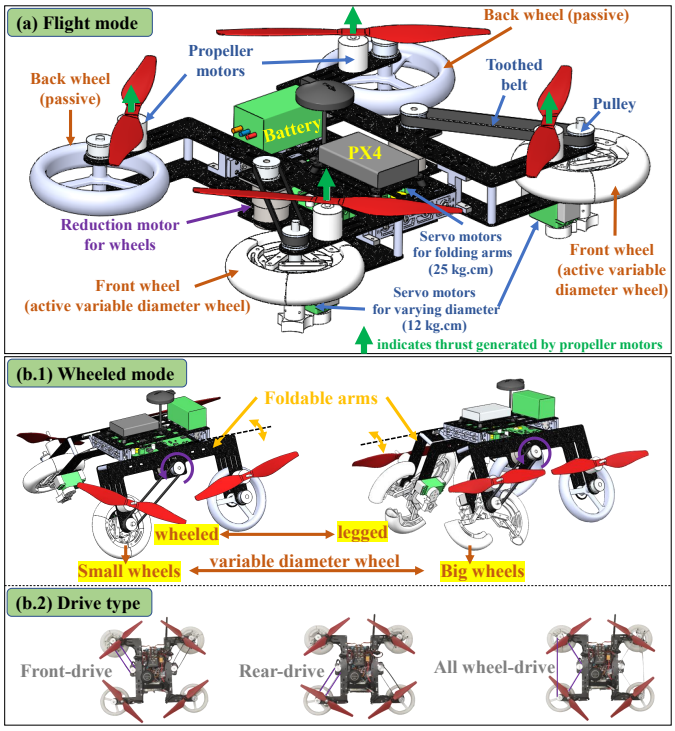


Fig. 2. The mechanism design of the multi-modal robot: (a) flying mode, (b.1) wheeling mode, and (b.2) drive type.

## II. Robot's Design

As the primary goal of this proposed robot is to realize multi-modal motion, including flight mode and wheeled mode, this section first provides an overview of the system design and then describes the working principle of the robot in flight mode and wheeled mode in terms of mechanism, actuation, and control.

### A. System overview

Fig. 2 demonstrates the overall design of the robot in flight mode and wheeled mode. The first mode is a conventional quadrotor with thrust provided by four propeller motors, see Fig. 2(a), and the second mode is a mobile robot with four wheels, see Fig. 2(b.1). The robot has a rigid core equipped with electronics including controllers for flight and wheels, propeller motors, servo motors, reduction motors, and battery, two foldable arms located on the left and right sides of the body, a pair of fixed-diameter wheels as the rear wheels, and a pair of variable-diameter wheels as the front wheels, which are designed to improve the traveling capabilities of the robot in wheeled mode.

Besides, the reduction motors that drive the wheeled motion are designed located in the middle of the left and right sides so that the wheels can be preset to front-drive, rear-drive, and four-wheel drive, as shown in Fig. 2(b.2), depending mainly on which wheels the belt is connected to. Fig. 2(b.1) illustrates an example of front-wheel drive, where the reduction motor drives the front wheels via a belt. It is noted that in this study, to ensure the stability of the quadrotor during flight, we do not allow arms to fold in the air. Therefore, there is no difference between the robot's flight mode from a conventional quadrotor, and the wheeled modal mechanism is mainly described below.

### B. Mechanism of the robot in wheeled mode

There are two key points in the design of the wheeled robot in this paper, one is to change from the horizontal state of the quadrotor to the folded arm state, which is generated by folding arms, and the other is to endow the wheels with the function of varying size, which is achieved by the variable-diameter wheels.

*1) Mechanism of foldable arms:* Two foldable arms are symmetrically distributed on both sides of the robot and actuated by the same servo motor located at the center of the robot. When the robot lands in a quadrotor shape, the corresponding arm is in a fully horizontal state, and then by controlling the angle between the folding arm and the horizontal line during the downward rotation of the folding arm, the transition of the flight mode to wheeled mode can be achieved. Conversely, the arms rotate upwards.

*2) Mechanism of variable-diameter wheels:* The variable-diameter wheel is designed based on the straight scissor element (SSE), which has been used in many applications such as bioinspired crawling robots [24], [25] and morphing quadrotors [26], [27] due to its advantages of combining large morphing ratio with high stiffness characteristics as well as the single degree of freedom thus easy to be controlled. The size of the wheels can be adjusted by changing the angle between two articulated scissors and the size of the scissor's bar length. More importantly, in the process of changing the wheel's size, the model of the wheel has also switched from continuous wheeled mode to legged mode, thus giving legged robots the ability to cross obstacles. It is worth mentioning that although all four wheels can be designed as variable-diameter wheels, to save extra weight for flying in flight mode, we only equipped the front wheels with variable-diameter wheels, see Fig. 2(b.1).

### C. Actuation and control

As depicted in Fig. 3, the robot is powered by a 4S Lipo battery for thrust generated by four propeller motors (2216 KV950), controlled by the PX4 through ESCs in flight mode. The total voltage splits two voltages through different step-down regulators, 6.8V for the servomotors (25 kg·cm) used to actuate the foldable arms, and 12V for the ROS robot controller to drive the active wheels using two reduction motors (reduction ratio of 1:56), and the 5V output of the ROS board is used to power the servo motors (12 kg·cm), which is designed for varying the size of the wheels.

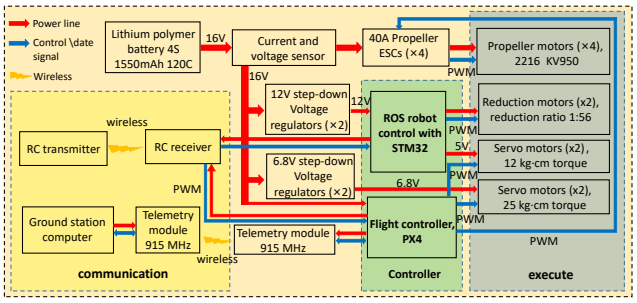


Fig. 3. The architecture of the proposed robot's electronics, communication, and controller.

## III. Kinematic Modeling of the Robot

Corresponding to the aforementioned robot's design, we mainly focus on the kinematics of the robot in wheeled mode in this section and evaluate the corresponding theoretical morphing performance of the foldable arms and variable-diameter wheels. Fig. 4 illustrates the schematic diagram for analyzing the kinematics.

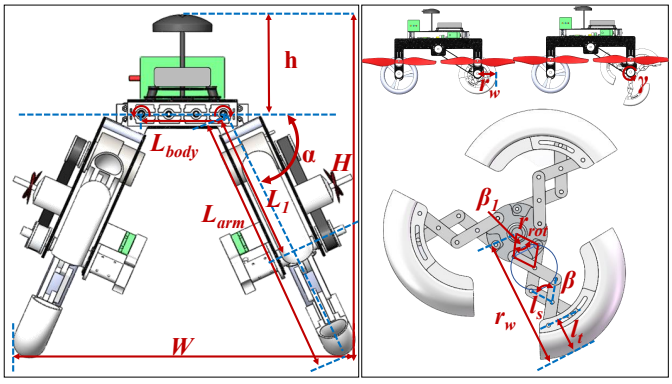


Fig. 4. Schematic diagram of kinematic analysis. $W$, $H$, and $r_w$ are the robot's width, height, and radius of the wheel, respectively.

### A. Kinematic analysis of foldable arms

*1) Robot's geometry associated with foldable arms:* Define $L_{body}$ as the constant length of the core body, $L_{arm}$ as the distance between the core body and the edge of the wheel, $h$ as a constant distance between the core body and the top of the robot, and $\alpha$ as the deployment angle of foldable arms, which is the acute angle of the plane on which the wheel is located and the plane in which the core body is located. Therefore, the length and width of the robot during the folding/unfolding process of the arm can be expressed as

$$\begin{aligned} W &= L_{body} + 2L_{arm}\cos\alpha \\ H &= h + L_{arm}\sin\alpha \end{aligned} \tag{1}$$

*2) Robot's modal transition performance associated with foldable arms:* The foldable arm is very important for realizing the modal transition between the flight mode and wheeled mode, and its folding performance directly determines how fast the modal transformation can be achieved.

The following briefly analyzes the foldable arm's angular velocity to evaluate modal transition performance.

The theoretical angular velocity of the foldable arm can be represented by $\dot{\alpha}$, whereas the corresponding actual values under different payloads need to be acquired based on experimental measurements. Even so, we can get the range of angular velocities by measuring the folding arm at no load and full load. It is known that the angular velocity of the servo motor that actuates the foldable arm without extra load is 0.17s/60°, and we also measured the angular velocity under full load, which is 0.9s/90°. Define $\omega_{arm}$ as the angular velocity of the foldable arms, thus we have $\omega_{arm} \in$[1.74, 6.16] rad/s, which can be regarded an index to evaluate the modal transition performance.

### B. Kinematic analysis of variable-diameter wheel

As shown in the right image in Fig. 4, $\beta$ is the deployment angles of the scissor elements with the bar length of $l_s$. According to the geometric relationship during the deployment of scissors, we can write the wheel's radius.

$$r_w = r_{rot}\cos\frac{\beta_1}{2} + 2nl_s\cos\frac{\beta}{2} + l_t \tag{2}$$

where

$$\beta_1 = 2\arccos\frac{\sqrt{r_{rot}^2 - (l_s\sin\frac{\beta}{2})^2}}{r_{rot}},$$

$n$ denotes the number of SSEs, $r_{rot}$ is the radius of the wheel's central rotational plate, and $l_t$ denotes the length of the wheel's thickness. $r_{rot}$ and $l_t$ are constants.

With (2) and the relationship between $L_{arm}$ and $r_w$, that is $L_{arm} = L_1 + r_w$, where $L_1$ represents the distance between the center of the hub and the core body, we can rewrite (1) as

$$W = \underline{L_{body}} + 2(\underline{L_1} + \underline{r_{rot}}\cos\frac{\beta_1}{2} + 2n\underline{l_s}\cos\frac{\beta}{2} + \underline{l_t})\cos\alpha, \tag{3}$$

and

$$H = \underline{h} + (\underline{L_1} + \underline{r_{rot}}\cos\frac{\beta_1}{2} + 2n\underline{l_s}\cos\frac{\beta}{2} + \underline{l_t})\sin\alpha, \tag{4}$$

where the constant variables are underlined.

Besides, the running speed of the robot can be described as

$$V = \omega_{wheel} r_w \tag{5}$$

where $\omega_{wheel}$ is the wheel's angular velocity, which is determined by the reduction motor.

It can be concluded from (3) and (4) that the geometry of the robot can be adjusted through the deployment angle of foldable arm $\alpha$ and the angle of SSEs $\beta$, which provides more options than a method with only one adjustable parameter. More than that, the number of SSEs can be changed to further adjust the robot's morphology to improve the obstacle-crossing performance. From (5), it can be drawn that the running speed of the robot can be improved by changing the radius in addition to the angular speed of the reduction motor, to improve the motion performance of the robot.

TABLE I
THE MASS DISTRIBUTION OF THE PROTOTYPE

| Main component | Mass |
|---|---|
| Core body | 400 g |
| Battery | 185 g |
| Propeller& motors&ESC (×4) | 417 g |
| Actuator control system | 174 g |
| Main accessories | 394 g |
| Servo motors 25kg·cm (×2) | 141 g |
| Reduction motors (x2) | 310 g |
| Toothed belt(×2)&Pulleys | 136 g |
| Passive fixed wheel(×2) | 78 g |
| Servo motors 12kg·cm (×2) | 97 g |
| Active variable-diameter wheel(×2) | 240 g |
| Total mass | 2572 g |

## IV. EXPERIMENTS AND RESULTS

To test the performance of the proposed robot, we manufactured the prototype by adopting a combination of 3D printing and machining technologies. The body's main structure is machined with carbon fiber to reduce the total weight, the joints that need to bear heavier loads are made of metal, and the non-load-bearing parts are 3D printed with strong plastic materials. The prototype is 2.57 kg in total, with the distribution listed in Tab. I, where the inherent weight of the robot designed for flying accounts for 61%, the weight used for enabling wheeled function accounts for 26%, and that for variable-diameter wheels is 13%. As the robot's flight mode is consistent with a regular quadrotor, we mainly introduce the tests on the response of foldable arms and variable-diameter wheels under payload, as well as the traveling performance of the robot in wheeled mode in the following experiments.

### A. Response performance tests of foldable arms and variable-diameter wheels

*1) Foldable arms:* Fig. 5(a) demonstrates the experimental setup for testing the response of the foldable arms under real payload. The robot was mounted on a fixed platform during the tests to ensure two arms rotated freely. The arm was driven by the servo motor through PWM to fold within a range. A motion camera was used to track the change of the deployable angle $\alpha$. The result in several repeatable cycles is plotted in Fig. 5(a.1), where a range of $0 \sim 65°$ was achieved as expected. During the test, since the inner parts of the two hubs occupy a certain amount of space, the foldable angle $\alpha$ can not reach the range of $66 \sim 90°$, but $65°$ is enough as a larger deployable angle may cause the body to roll over. In regular wheeled mode, the angle $\alpha$ is set to be around $45°$.

*2) Variable-diameter wheels:* Fig. 5(b) demonstrates the experimental setup for testing the response of the variable wheel. Similarly, the robot was mounted on a fixed platform to ensure the wheels changed size freely. A motion camera was used to track the change of the deployable angle of the pair of scissors $\beta$ and the radius of the wheel $r_w$. A ruler was placed in the plane on which the wheel was located for calibration. The results in several repeatable cycles are plotted in Fig. 5(b.1) and (b.2), where the radius of the wheel

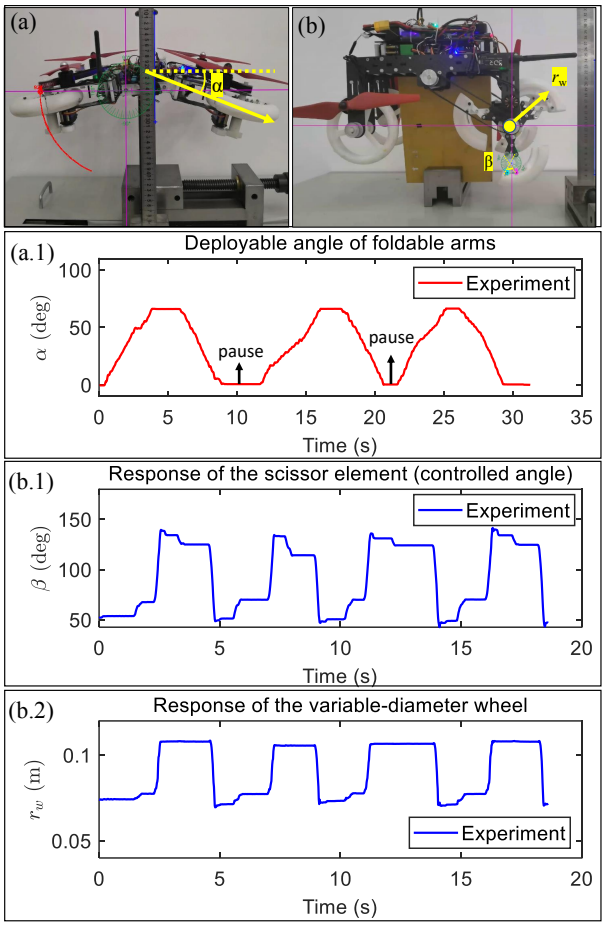


Fig. 5. Experimental setup (a) and (b), and results of testing the folding arms and variable-diameter wheels. (a.1) corresponding to (a), and (b.1) and (b.2) corresponding to (b).

$r_w$ varies from 0.065 m to 0.11 m with $\beta$ changes from $[49, 113°]$.

### B. Traversal performance tests of the robot

*1) Obstacle avoidance performance:* To reduce the times of "have to take off for obstacle avoidance", which is the obstacle avoidance strategy currently adopted by many multimodal robots, our robot allows more obstacle avoidance strategies in its wheeling mode to enhance its traversal performance. Fig. 6 representatively demonstrates the robot's reaction when faced with different types of obstacles. Fig. 6(a) shows the scenario of the narrow and high space that robots often encounter in reality, at which point the robot folds both arms to reduce the body's width until it is less than the width of the obstacle. Conversely, Fig. 6(b) shows a short and wide scene, where the robot's body is folded to reduce its width if it is in quadrotor shape; in the opposite, if the robot is in wheeled mode, it will spread its body as flat as possible and lower its height to pass an obstacle with a width of 45 cm and a height of 20 cm. The above two obstacle avoidance abilities are achieved simply by folding the arms. Accordingly, the changes in width and height are plotted in the first two plots in Fig. 6(d).

Fig. 6(c) shows an example of obstacle avoidance by

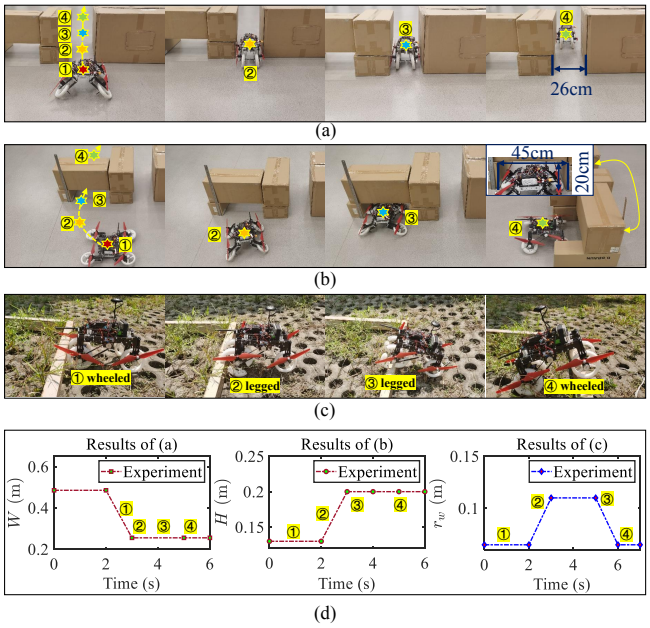


Fig. 6. Obstacle avoidance demonstration of the robot in wheeling mode by folding arms for the traversal of narrow passageways (a) and (b), or varying diameter for obstacle-crossing (c), and the results (d) corresponding to (a)∼(c).

adjusting the wheels' size. In this case, the robot can achieve the ability to cross a stair by changing the diameter of the wheel, turning the original small wheel into a large wheel, and transitioning from wheeled mode to legged mode. Accordingly, the change in the diameter is plotted in the final plot in Fig. 6(d).

*2) Climbing performance:* To test the climbing performance of the robot, we placed the robot on slopes with different inclinations, as shown in Fig. 7. The robot's wheels are made of resin material, and the contact inclined surface is made of rubber. During the test, the robot started from a flat ground and moved in a wheeled mode, climbing up a slope until it reached a high flat terrace. During this process, the slope angle was monitored using a protractor.

Fig. 7 demonstrates several captured images of the robot at different slopes, including 15°, 20°, 25°, 30° and 35°. The experimental results reveal that in the combination of resin-rubber, the maximum slope the robot can climb is 36°. This inclination can be enhanced by changing the material of the wheels.

*3) Tests on different terrains:* In addition to the advantages of folding arms and large diameters shown above, we further tested the robot's performance with small wheels in different terrains such as paved roads, meadows, gravel roads, and sewer grille ground in the state of small wheels (see the supplementary video). On a relatively flat road, the measured motion speed of the robot with small wheels is 1.1 m/s. Tab. II illustrates the main specifications of the robot.

## V. Conclusion

In this paper, we presented a novel multimodal robot that can fly like conventional quadrotors and crawl like wheeled robots. To achieve the transition between modes,

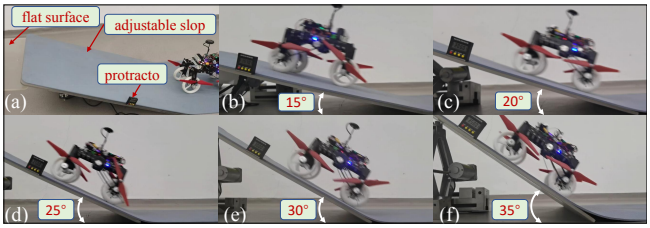


Fig. 7. Testing the climbing performance of the robot on the slopes with different inclinations.

TABLE II

THE MAIN SPECIFICATIONS OF THE PROTOTYPE

| | |
|---|---|
| Arm folding angle | $0° \leq \alpha \leq 65°$ |
| Scissor angle | $49° \leq \beta \leq 113°$ |
| Robot size ($\alpha$=0, excluding GPS) | 485 mm ×390 mm×130 mm |
| Wheel's size | 65 mm $\leq r_w \leq$ 110 mm |
| Average speed on flat ground | 1.1 m/s |
| Maximum climbing angle (resin-rubber) | 36° |
| Minimum traversal width | 255 mm |
| Minimum traversal height | 205 mm |
| Instantaneous current (wheeled mode) | 0.2 A |
| Instantaneous current (folding) | 2 A |
| Instantaneous current (varying diameter) | 0.9 A |

we designed a pair of foldable arms, which can complete a one-time folding within 0.9 s. Advanced on the wheeled robot, our robot has two variable-diameter wheels as the front wheels that were designed to further enhance the traveling capabilities in wheeled mode. Experiments have shown that the prototype has more options to tackle obstacles. Compared with the current takeoff obstacle avoidance strategy, obstacle avoidance can also be achieved by folding the arm or adjusting the wheel size in the wheeled mode, improving the traversal performance of the multi-modal robot. Our next work includes testing the performance of modal-transition and optimizing the variable-diameter wheel to implement a wheel with a greater morphing ratio, and to equip the prototype with more sensors, such as distance sensors and cameras, to enable autonomous decision-making between modalities.

## REFERENCES


[1] B. J. Emran and H. Najjaran, "A review of quadrotor: An underactuated mechanical system," *Annual Reviews in Control*, vol. 46, pp. 165–180, 2018.

[2] J. Ni, J. Hu, and C. Xiang, "Robust control in diagonal move steer mode and experiment on an x-by-wire ugv," *IEEE/ASME Transactions on Mechatronics*, vol. 24, no. 2, pp. 572–584, 2019.

[3] N. Meiri and D. Zarrouk, "Flying star, a hybrid crawling and flying sprawl tuned robot," in *2019 International Conference on Robotics and Automation (ICRA)*, pp. 5302–5308, IEEE, 2019.

[4] K. Patnaik and W. Zhang, "Towards reconfigurable and flexible multirotors: A literature survey and discussion on potential challenges," *International Journal of Intelligent Robotics and Applications*, vol. 5, no. 3, pp. 365–380, 2021.

[5] E. Sihite, A. Kalantari, R. Nemovi, A. Ramezani, and M. Gharib, "Multi-modal mobility morphobot (m4) with appendage repurposing for locomotion plasticity enhancement," *Nature communications*, vol. 14, no. 1, p. 3323, 2023.

[6] N. B. David and D. Zarrouk, "Design and analysis of fcstar, a hybrid flying and climbing sprawl tuned robot," *IEEE Robotics and Automation Letters*, vol. 6, no. 4, pp. 6188–6195, 2021.

[7] E. Gefen and D. Zarrouk, "Flying star2, a hybrid flying driving robot with a clutch mechanism and energy optimization algorithm," *IEEE Access*, vol. 10, pp. 115491–115502, 2022.

[8] T. Dias and M. Basiri, "Bogiecopter: A multi-modal aerial-ground vehicle for long-endurance inspection applications," *arXiv preprint arXiv:2303.01933*, 2023.

[9] A. Kalantari and M. Spenko, "Design and experimental validation of hytaq, a hybrid terrestrial and aerial quadrotor," in *2013 IEEE International Conference on Robotics and Automation*, pp. 4445–4450, 2013.

[10] Q. Tan, X. Zhang, H. Liu, S. Jiao, M. Zhou, and J. Li, "Multimodal dynamics analysis and control for amphibious fly-drive vehicle," *IEEE/ASME Transactions on Mechatronics*, vol. 26, no. 2, pp. 621–632, 2021.

[11] S. Mintchev and D. Floreano, "A multi-modal hovering and terrestrial robot with adaptive morphology," in *Proceedings of the 2nd International Symposium on Aerial Robotics*, no. CONF, 2018.

[12] A. Kalantari, T. Touma, L. Kim, R. Jitosho, K. Strickland, B. T. Lopez, and A.-A. Agha-Mohammadi, "Drivocopter: A concept hybrid aerial/ground vehicle for long-endurance mobility," in *2020 IEEE Aerospace Conference*, pp. 1–10, IEEE, 2020.

[13] J. Yang, Y. Zhu, L. Zhang, Y. Dong, and Y. Ding, "Sytab: A class of smooth-transition hybrid terrestrial/aerial bicopters," *IEEE Robotics and Automation Letters*, vol. 7, no. 4, pp. 9199–9206, 2022.

[14] K. Kim, P. Spieler, E.-S. Lupu, A. Ramezani, and S.-J. Chung, "A bipedal walking robot that can fly, slackline, and skateboard," *Science Robotics*, vol. 6, no. 59, p. eabf8136, 2021.

[15] S. Morton and N. Papanikolopoulos, "A small hybrid ground-air vehicle concept," in *2017 IEEE/RSJ International Conference on Intelligent Robots and Systems (IROS)*, pp. 5149–5154, IEEE, 2017.

[16] N. Pan, J. Jiang, R. Zhang, C. Xu, and F. Gao, "Skywalker: A compact and agile air-ground omnidirectional vehicle," *IEEE Robotics and Automation Letters*, vol. 8, no. 5, pp. 2534–2541, 2023.

[17] X. Shi, K. Kim, S. Rahili, and S.-J. Chung, "Nonlinear control of autonomous flying cars with wings and distributed electric propulsion," in *2018 IEEE Conference on Decision and Control (CDC)*, pp. 5326–5333, IEEE, 2018.

[18] R. Zhang, Y. Wu, L. Zhang, C. Xu, and F. Gao, "Autonomous and adaptive navigation for terrestrial-aerial bimodal vehicles," *IEEE Robotics and Automation Letters*, vol. 7, no. 2, pp. 3008–3015, 2022.

[19] A. Tagliabue, S. Schneider, M. Pavone, and A.-a. Agha-mohammadi, "Shapeshifter: A multi-agent, multi-modal robotic platform for exploration of titan," in *2020 IEEE aerospace conference*, pp. 1–13, IEEE, 2020.

[20] B. Araki, J. Strang, S. Pohorecky, C. Qiu, T. Naegeli, and D. Rus, "Multi-robot path planning for a swarm of robots that can both fly and drive," in *2017 IEEE International Conference on Robotics and Automation (ICRA)*, pp. 5575–5582, IEEE, 2017.

[21] R. J. Bachmann, F. J. Boria, R. Vaidyanathan, P. G. Ifju, and R. D. Quinn, "A biologically inspired micro-vehicle capable of aerial and terrestrial locomotion," *Mechanism and Machine Theory*, vol. 44, no. 3, pp. 513–526, 2009.

[22] R. Baines, S. K. Patiballa, J. Booth, L. Ramirez, T. Sipple, A. Garcia, F. Fish, and R. Kramer-Bottiglio, "Multi-environment robotic transitions through adaptive morphogenesis," *Nature*, vol. 610, no. 7931, pp. 283–289, 2022.

[23] S. J. Kerr, F. E. Fish, A. J. Nicastro, J. A. Zeligs, S. Skrovan, and M. C. Leftwich, "Biomechanical energetics of terrestrial locomotion in california sea lions (zalophus californianus)," *Journal of Experimental Biology*, vol. 225, no. 18, p. jeb244163, 2022.

[24] Y. Luo, N. Zhao, K. J. Kim, J. Yi, and Y. Shen, "Inchworm locomotion mechanism inspired self-deformable capsule-like robot: Design, modeling, and experimental validation," in *IEEE International Conference on Robotics and Automation (ICRA)*, pp. 6800–6805, IEEE, 2018.

[25] N. Zhao, Y. Luo, and Y. Shen, "Design, modeling and validation of a deformable capsule-like crawling robot based on scissor elements," *Mechanism and Machine Theory*, vol. 181, p. 105173, 2023.

[26] N. Zhao, W. Yang, C. Peng, G. Wang, and Y. Shen, "Comparative validation study on bioinspired morphology-adaptation flight performance of a morphing quad-rotor," *IEEE Robotics and Automation Letters*, vol. 6, no. 3, pp. 5145–5152, 2021.

[27] N. Zhao, Y. Luo, H. Deng, and Y. Shen, "The deformable quadrotor: Design, kinematics and dynamics characterization, and flight performance validation," in *2017 IEEE/RSJ International Conference on Intelligent Robots and Systems (IROS)*, pp. 2391–2396, IEEE, 2017.